Global dynamics and stochastic resonance of the forced FitzHugh-Nagumo neuron model

Pu-Lin Gong and Jian-Xue Xu
School of Civil Engineering and Mechanics, Xi'an Jiaotong University, Xi'an 710049, People's Republic of China
(Received 28 September 1999; revised manuscript received 28 November 2000; published 26 February 2001)

We have analyzed the responses of an excitable FitzHugh-Nagumo neuron model to a weak periodic signal with and without noise. In contrast to previous studies which have dealt with stochastic resonance in the excitable model when the model with periodic input has only one stable attractor, we have focused our attention on the relationship between the global dynamics of the forced excitable neuron model and stochastic resonance. Our results show that for some parameters the forced FitzHugh-Nagumo neuron model has two attractors: the small-amplitude subthreshold periodic oscillation and the large-amplitude suprathreshold periodic oscillation. Random transitions between these two periodic oscillations are the essential mechanism underlying stochastic resonance in this model. Differences of such stochastic resonance to that in a classical bistable system and the excitable system are discussed. We also report that the state of the basin of attraction has a significant effect on the stability of neuronal firings, in the sense that the fractal basin boundary of the system enhances the noise-induced transitions.

DOI: 10.1103/PhysRevE.63.031906 PACS number(s): 87.10.+e, 05.40.−a, 87.19.La

I. INTRODUCTION

Excitable dynamics underlie the behavior of many systems ranging from Josephson junction to chemical reactions to cardiac and nerve cells. In these systems a large perturbation can elicit a large amplitude spike or ''firing,'' followed by a quick return to a globally attracting fixed point. The dynamical response of these systems to the periodic deterministic forcing has been extensively described in both experimental and model studies [1,2]. As a simple but representative example of excitable systems, the Fitzhugh-Nagumo (FHN) neuron model was originally suggested for the description of firing behaviors of sensory neurons [3]; it was also widely used for the modeling of a spiral wave in a two-dimensional excitable medium. The detailed phase-locking dynamics of the periodically stimulated FHN equation has been investigated [4]. Recently, the forced FHN neuron model with noise input has been studied to reveal how information is encoded and transmitted in a neuron system under noisy circumstance [5–10]. It was found that, in this typical excitable neuron model, noise can enhance the detection of weak subthreshold signals using the mechanism of stochastic resonance. Coherence resonance was also found in the noisy neuron model [11]. In the classical stochastic resonance theory, stochastic resonance is related to random transitions from one stable equilibrium state to the other. As for the previous studies about stochastic resonance in the excitable FHN model, although the forced excitable model has only one attractor, it has been found that the histogram of the interspike intervals has a multimodel structure with the peaks located at integer multiples of the driving period, and stochastic resonance still occurs in the excitable neuronal model. But for the excitable FHN neuron model it still remains unclear whether stochastic resonance is related to bistability. Moreover, the coexistent attractors have been observed experimentally in real excitable neurons [12–14]. Therefore to understand stochastic resonance in these neuronal systems, it is necessary to study whether stochastic resonance in the excitable neuron model is related to bistability. In this paper we present a global view of the periodic solutions of the FHN neuron model with weak periodic stimulation in the two-parameter space. Then we pay attention to the parameter regions associated with the bistability in the periodically forced FHN neuron model and study how noise-induced random transitions between the bistability are related to stochastic resonance in the excitable neuron model. In the previous studies about the stability of firing activity in some neuron models [15], little attention has been paid to the global dynamics of these systems. Furthermore, it has been regarded that the information concerning the neuron's input may be encoded in the interspike intervals of neuron firings [16,17]. A precondition of the code manner is that the firings of the response to an input signal be stable in the presence of noise [18]. So, when multiple steady states coexist in the excitable neuron model, we should discuss whether the global dynamics of the typical neuron model have effects on the stability of neuronal firings under noise perturbations.

With these aims in the view, the paper is organized in the following manner. The bistability and stochastic resonance are the subjects of Sec. II. In Sec. III we study the relationship between the state of basin and the stability of the firing state. At the end of the paper some conclusions are drawn.

II. BISTABILITY OF THE FORCED FHN NEURON MODEL AND STOCHASTIC RESONANCE

A. The global dynamics of the forced FHN neuron model

We consider the periodically forced FitzHugh-Nagumo neuron model in the following form:

$$\varepsilon \frac{dv}{dt} = v(v-a)(1-v) - w,$$
$$\frac{dw}{dt} = v - dw - b + r\sin(\beta t). \tag{1}$$

The variable v is the fast voltagelike variable and w is the slow recovery variable. Throughout the paper we fix the val-

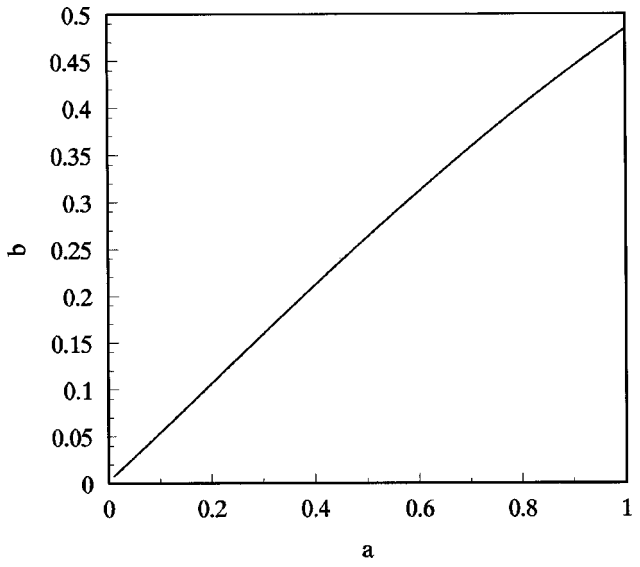

FIG. 1. The Hopf bifurcation points in parameter space *a*-*b*. The units of *a* and *b* are arbitrary.

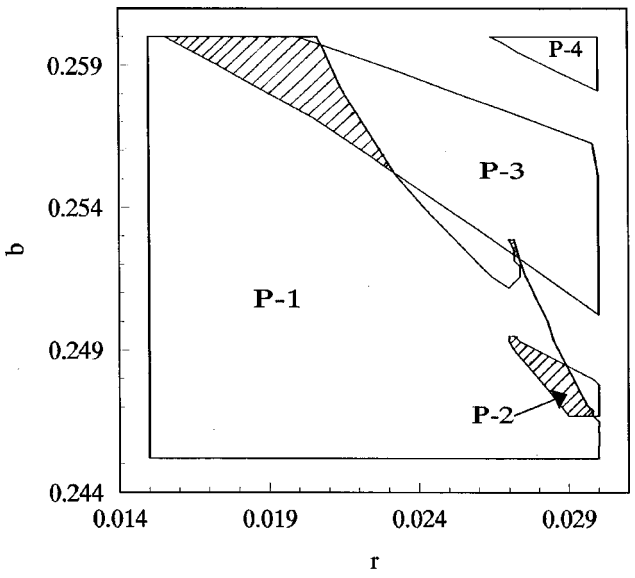

FIG. 2. The periodic solutions of the forced FHN neuron model in the parameter plane *r*-*b*. The dominant mode-locking regions are marked by *P*-*k*, $k=1,2,3,4$. In the crossing regions shaded by the solid lines, the forced neuronal model has coexistent attractors. The units of the *r* and *b* are arbitrary.

ues of the constants to $\varepsilon=0.005$, $d=1.0$, and $\beta=7.5$. A firing or a spike is considered to occur if the variable v has a positive-going crossing of the firing threshold v_{th}, chosen as $v_{\mathrm{th}}=0.5$. Here the slow variable of the neuronal model is driven by the external weak signal, the reason for this is to allow comparison with the results obtained by other scholars [4–6], in their studies the slow variable was also driven by the external periodic signal. For the unforced FHN equation, i.e., in Eq. (1) $r=0$, the system has equilibrium (v_0,w_0), where v_0 is real-valued root of $v_0(v_0-a)(1-v_0)=v_0-b$, and $w_0=v_0-b$. The stability of the equilibrium point is determined by the Jacobian matrix

$$D=\begin{pmatrix} (-3v_0^2+2(1+a)v_0-a)/\varepsilon & -/\varepsilon \\ 1 & -1 \end{pmatrix}.$$

In the *a*-*b* parameter space, from the condition for the existence of a Hopf bifurcation [19], we obtain that the unforced system has Hopf bifurcation when parameters *a* and *b* satisfy the following algebraic equation:

$$b=\frac{1+a}{3}-\frac{c}{60}-\left(\frac{1+a}{3}-\frac{c}{60}\right)\left(\frac{1-2a}{3}-\frac{c}{60}\right)\left(\frac{2-a}{3}+\frac{c}{60}\right), \tag{2}$$

where $c=\sqrt{394-400a+400a^2}$. The Hopf bifurcation points satisfying Eq. (2) are shown in Fig. 1. In the following studies the value of parameter *a* is fixed to $a=0.5$. For this case, the stability check of the equilibrium shows that when $b<0.2623$ the unforced FHN neuron model has only one stable equilibrium, and at $b=0.2623$ a supercritical Hopf bifurcation occurs. For $b>0.2623$, the unforced model has a stable limit cycle.

In the present studies we consider the case of $b<0.2623$, the unforced neuron model has only one stable equilibrium, it is excitable and related to the physiological situation of some excitable neurons. When a very weak periodic stimulation is forced on the excitable system [in Eq. (1) $r>0$], the global dynamic characteristics of the system within the parameter region $b1<b<b2, r1<r<r2$ will be studied, where $b1=0.245$, $b2=0.26$, $r1=0.015$, and $r2=0.03$. For this purpose we first integrate Eq. (1) by setting *b* to a certain value and increasing *r* from $r1$ to $r2$, and then decreasing from $r2$ to $r1$ in a step of 0.0002. In this process, the final point of the last computed stable solution is always used as an initial point for the new computation. After this process, the characteristics of the stable solution on a straight line in the (b,r) plane with $b=$constant may be determined. We then increase *b* with a step of 0.0002, and repeat the above procedure to find the characteristics of solutions of Eq. (1) on another straight line with $b=$constant. In this way, the diagram in the parameter space that summarizes the results of the calculation can be drawn and shown in Fig. 2. In Fig. 2 the region marked by *P*-*k* represents that, when the parameters *b* and *r* fall into this region, the system has a stable periodic orbit with the period of $T=kT_0$, $T_0=2\pi/\beta=0.837$. In the present studies we only focus our attention on the low-order periodic solutions *P*-*k*, $k=1,2,3,4$. As shown in Fig. 2, there exist the crossing regions which are shadowed by the solid lines, in these regions different periodic orbits coexist at the same parameter values. We also illustrated the simultaneous existence of the attractors by choosing some different initial points. In [20,21], the Borhoeffer Van der Pol system, which is a FHN-type model, has been studied. The quasiperiodic, chaotic motion were found for some parameters. Other nonlinear phenomena such as crisis, intermittency, and bistability were also found in the forced Borhoeffer Van der Pol system. In this paper we present a global view of the periodic solutions of the periodically forced FHN neuron model in the two-dimensional parameter space.

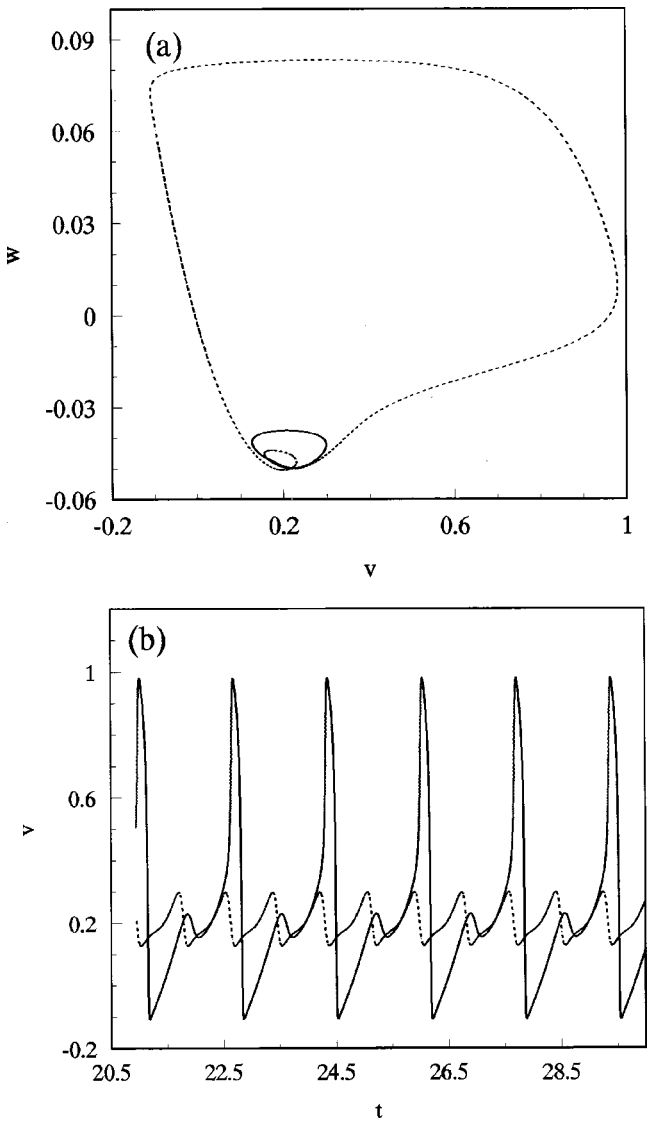

FIG. 3. The subthreshold small-amplitude periodic solution with period $T_1=T_0$ and the suprathreshold large-amplitude periodic solution with period $T_2=2T_0$: (a) the coexistent attractors in the state space v-w, the dashed line is for the suprathreshold oscillation and the solid line is for the subthreshold oscillation; (b) Membrane potential v versus time t for the two attractors, the dashed line is for the subthreshold oscillation and the solid line is for the suprathreshold oscillation. The units of the v, w, and t are arbitrary.

As shown in Fig. 2, the coexistent attractors are very common in the chosen parameter region. In the crossing regions shadowed by the solid lines, we choose the parameters $b=0.2466$, $r=0.0292$. We checked that for some parameters in the shadowed regions of Fig. 2, similar results could be obtained as those shown below for the case of $b=0.2466$, $r=0.0292$. When $b=0.2466$, $r=0.0292$, the forced neuron model has two globally stable attractors, one is the subthreshold small-amplitude periodic oscillation with period $T_1=T_0$, the other is the suprathreshold large-amplitude periodic oscillation with period $T_2=2T_0$. The coexistent periodic oscillations are shown in Fig. 3. Next let us consider the basin of attraction of the coexistent attractors. In the region

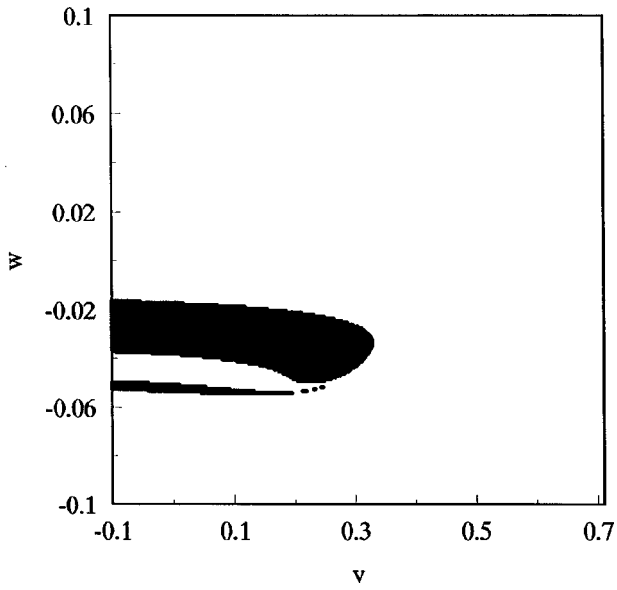

FIG. 4. Basin of attraction for the forced FHN neuronal model when $b=0.2466$, $r=0.0292$. The black dots represent the basin of attraction of the subthreshold oscillation, the other region is the basin of attraction of the suprathreshold oscillation. The units of v and w are arbitrary.

of phase space $-0.1<v<0.7, -0.1<w<0.1, 400\times200$ initial conditions are uniformly chosen in the form of grids and each of them is integrated to decide which attractors it eventually resides on. From the calculations, the basin of attraction in the chosen region of phase space can be obtained, which is shown in Fig. 4. If the initial state of the neuron model starts from the basin of attraction of the subthreshold periodic oscillation, the final state of the neuron model is the subthreshold oscillation, the neuron does not fire. On the other hand if the neuron model starts from the basin of attraction of the suprathreshold oscillation, the neuron model has the stable periodic firings pattern. The result shows that initial states also play an important role in the discharging behaviors of neurons. From the point of view of neuron firings, the external signal that can induce firings is regarded as a suprathreshold stimulation, otherwise it is a subthreshold stimulation. In the previous studies about stochastic resonance in some simple bistable systems and excitable neuron models, the external stimulation forced on these systems is a subthreshold input signal. However, for the case studied by us, when a weak periodic signal is forced on the FHN neuron which is in the excitable region, both the subthreshold oscillation and the suprathreshold oscillation can be generated simultaneously by the weak stimulation, thus the periodic signal can be regarded as a suprathreshold stimulation as well as a subthreshold stimulation.

B. Stochastic resonance related to the dynamic bistability

In the classical stochastic resonance theory, stochastic resonance (SR) phenomenon occurs in a bistable system which has two static fixed points [22–24]. For the previous studies about stochastic resonance in the excitable FHN neuronal model [5,25] we can verify that in their consideration

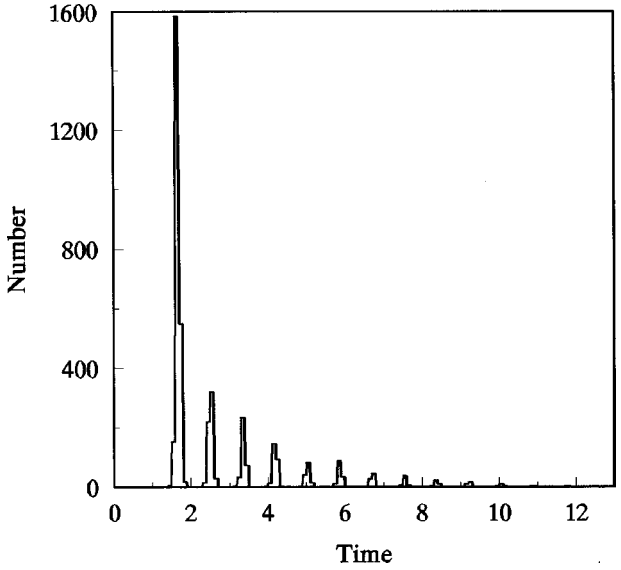

FIG. 5. The interspike intervals histogram when noise intensity $D=4\times10^{-7}$. The units of the axes are arbitrary.

the forced excitable FHN neuron model has only one attractor. However, as shown in the present study, the dynamic bistabilities (one is subthreshold oscillation and the other is the suprathreshold oscillation) are very common for the forced FHN neuronal model in some parameter regions. Therefore whether stochastic resonance occurs in these regions and is related to the coexistence of two attractors arises naturally in this context.

To address the question, white Gaussian noise $\xi(t)$ with the mean $\langle\xi(t)\rangle=0$ and the autocorrelation function $\langle\xi(t)\xi(s)\rangle=2D\delta(t-s)$ is added on Eq. (1):

$$\begin{aligned}\varepsilon\dot{v}&=v(v-0.5)(1-v)-w,\\ \dot{w}&=v-dw-b+r\sin(\beta t)+\xi(t),\end{aligned}\tag{3}$$

where $\varepsilon=0.005$, $d=1.0$, $\beta=7.5$, and $b=0.2466$, $r=0.0292$. We integrate Eq. (3) using the forth-order Runge-Kutta method with the time step of 0.001. For a fixed noise intensity, such as $D=4\times10^{-7}$, an initial point from the basin of attraction of the subthreshold oscillation is chosen. After discarding a long-time transient state, the histogram of interspike intervals is obtained and shown in Fig. 5. It has a multipeaked structure and the interval between these peaks is close to the period of the weak signal. In addition, the decay of the envelope of the interspike intervals histogram is indistinguishable from an exponential function, i.e., $A_{\max}\propto\exp(-\lambda_1 T)$ with the decay constant $\lambda_1=0.255$. The same histogram of the interspike intervals can be obtained by initiating the system within the basin of the suprathreshold oscillation. This signifies that the statistical characteristic of the interspike intervals is independent of initial conditions.

In the present studies the interspike interval histogram has a multipeaked structure and the interval between these peaks is close to the period of the weak signal, we wonder whether stochastic resonance occurs. First, we use the measure introduced in [26] to study whether stochastic resonance occurs,

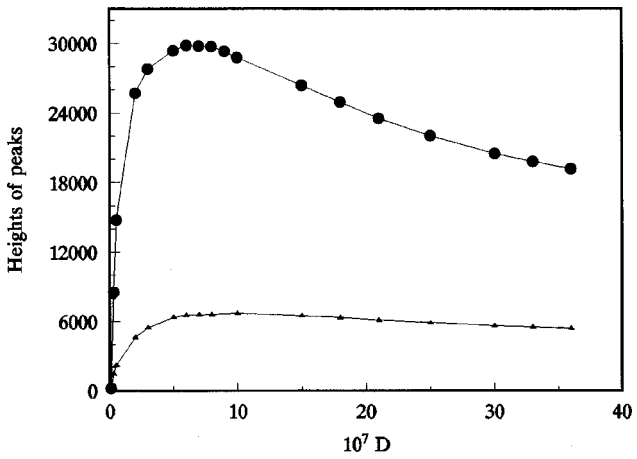

FIG. 6. Heights of the first (dots) and second (triangles) peaks of the difference of the interspike intervals histogram in the presence of periodic force and the interspike intervals histogram in the absence of periodic force versus noise intensity D. The units of the axes are arbitrary.

i.e., the difference of the interspike interval histogram in the presence of periodic force and the interspike interval histogram in the absence of periodic force. During the process of varying noise intensity, the behavior of the peak heights of the difference as a function of noise intensity D is shown in Fig. 6. It shows that the first peak and the second peak reach maximum values individually. This result indicates that stochastic resonance occurs in this case studies by us. Then, the signal-to-noise ratio is calculated by us. The power spectral density is calculated from the spike train through Fourier transform as in Ref. [10]. The signal-to-noise ratio is obtained from the power spectrum as $R_{\mathrm{SN}}=10\log_{10}[S(w)/N(w)]$, where R_{SN} is the signal-to-noise ratio, the signal power $s(w)$ is the height of the signal peak located at the signal frequency, and the noise power $N(w)$ is the amplitude of the background noise measured at the base of the signal peak. The signal-to-noise ratio as a function of noise intensity D is shown in Fig. 7. It increases with noise intensity D, reaches a maximum, and decreases again, displaying the typical feature of stochastic resonance.

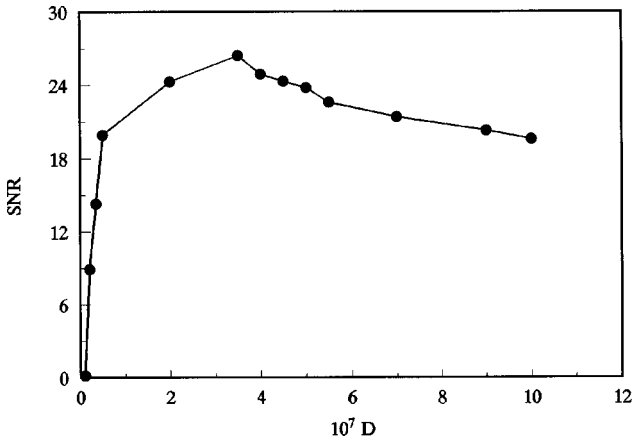

FIG. 7. Signal-to-noise ratios versus noise intensity D. The units of the axes are arbitrary.

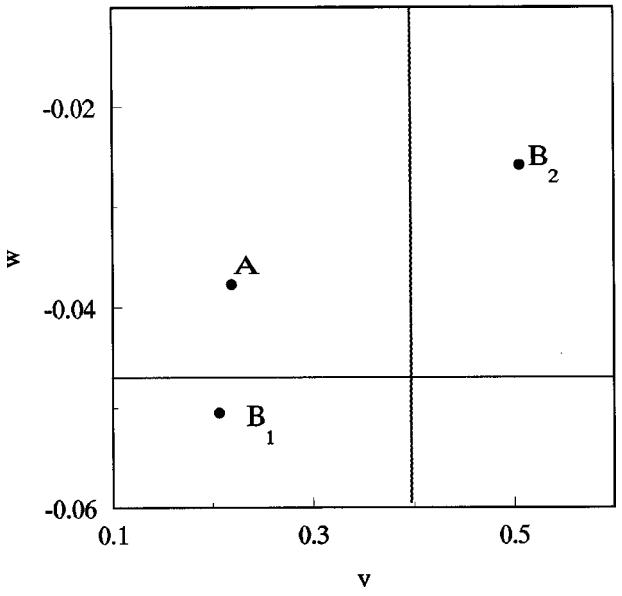

FIG. 8. The periodic orbits in Poincaré section, the parameter $a=0.2466$, $b=0.0292$. The units of the axes are arbitrary.

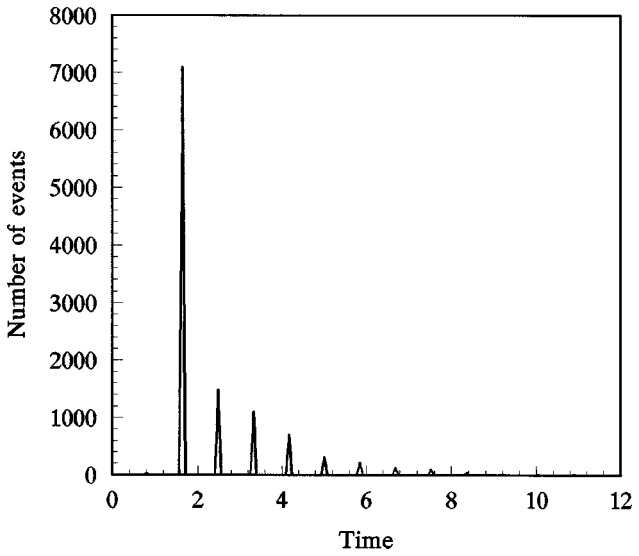

FIG. 9. The return-time distribution of the B_2 in Poicaré section when noise intensity $D=4\times10^{-7}$. The units of the axes are arbitrary.

To interpret the basic mechanism underlying stochastic resonance of the present study and show some differences between our case and the previous studies in a typical bistable system and the excitable system, we need to analyze the statistics of random jumps between these two coexisting attractors. However, as shown in Fig. 3(a), even in the absence of noise, the orbits of the two dynamic oscillations are very close to each other in phase space. Thus when in the presence of noise, it is very difficult to discern the detailed switching behaviors between the two attractors in phase space. To overcome this problem, we consider the switching behaviors induced by noise in the Poincaré section. In general, for a periodically forced nonlinear system $\dot{x}=f(x,t)=f(x,t+T)$, $x\in R^n$, where T is the period of an external force. If time is included as a explicit state variable:

$$\begin{matrix}\dot{x}=f(x,\theta)\\ \dot{\theta}=1\end{matrix}\qquad (x,\theta)=R^n\times S^1,$$

the Poincaré section Σ can be chosen as $\Sigma=\{(x,\theta)\in R^n\times S^1\theta=\pi\}$, the Poincaré map is given by $P:\Sigma\rightarrow\Sigma$ [19]. By this method we construct a Poincaré map for Eq. (1) with parameters $b=0.2466$, $r=0.0292$. Two coexistent periodic orbits for the Poincaré map can be obtained. One is the period-1 orbit that is shown in Fig. 8 as point A, the other is the period-2 orbit consisting of two points which are shown in Fig. 8 as points B_1 and B_2. The period-1 orbit and the period-2 orbit in the Poincaré section correspond to the subthreshold oscillation and the suprathreshold oscillation of the original continuous system, respectively. When noise is forced on the system [i.e., Eq. (3)], after discarding a long-time transient state, in the Poincaré section each point of the two periodic orbits is smeared and broadened around itself due to the random transitions induced by noise. For this reason, to study the random switching behaviors between the coexistent attractors in the Poincaré section, we divide the region around them into three subregions as shown in Fig. 8, which are marked by I, II, and III, respectively. As for each subregion, it is in the basin of attraction of its corresponding attractor. For period-1 orbit A, it is smeared and extended around itself by noise, but the extension of the point is confined to the subregion I around A. Therefore if a noisy orbit is mapped into the subregion I around A, we regard that it is switched to the period-1 orbit A. The same things occur for the point B_1 in subregion II and B_2 in subregion III as those for point A in subregion I.

Through studying the long-time random switching behaviors in the Poincaré section with the division mentioned above, we find that two features of these transitions are notable. First, if a point starts from subregion III around B_2, the following point is necessarily in subregion II around B_1. Second, there only exist two switching routes between these two coexistent attractors, that is, transition from subregion II around B_1 to subregion I around A and transition from subregion I around A to subregion III around B_2. In all cases we observe that a trajectory eventually settles into the region around one of the attractors known to exist in the absence of noise, no new stable state appears in this system as a consequence of noise. Noise only induces transitions between the two-coexisting attractors. Thus stochastic resonance studied here is related to random transitions between these two attractors.

We consider the return-time distribution for B_2 which is one branch of the period-2 orbit, e.g., the distribution of the time interval T it takes for the system to be first kicked from subregion III around B_2 to other subregions and back again. The histogram of the return time is shown in Fig. 9. This histogram is similar to the one shown in Fig. 5 for the original continuous noisy model. Further calculation shows that the decay of the envelope of the interspike interval histogram also satisfies $A_{\max}\propto\exp(-\lambda_2 T)$, with $\lambda_2=0.2542$ which is close to the decay constant λ_1 of the interspike intervals

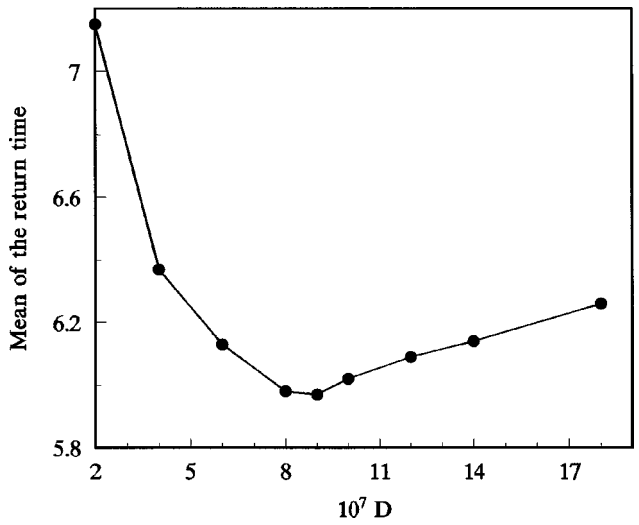

FIG. 10. Mean of the return time versus noise intensity D. The units of axes are arbitrary.

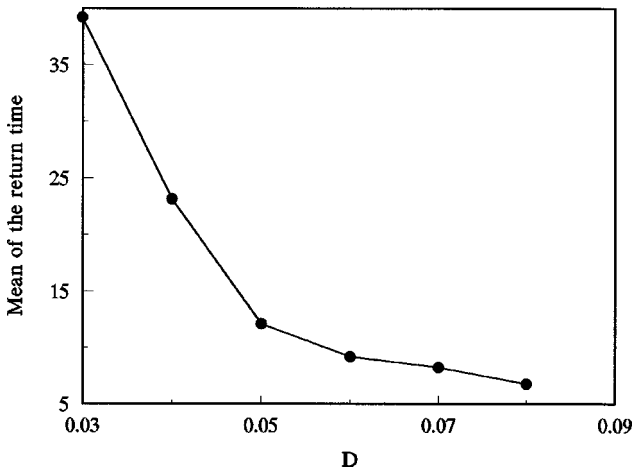

FIG. 11. Mean of the return time versus noise intensity D for the classical double-well system, the equation is $\dot{x}=x-x^3+a\sin(wt)+\xi(t)$, where $a=0.2$, $w=0.0314$, $\langle\xi(t)\rangle=0$, and $\langle\xi(t)\xi(s)\rangle=2D\delta(t-s)$. The units of the axes are arbitrary.

histogram shown in Fig. 5. The reason for this is that when an orbit is mapped into subregion III around B_2, it corresponds to the case that the original continuous noisy system can generate a spike. This also demonstrates that transitions induced by noise between these periodic orbits in the Poincaré section provide a good approximation of the switching behaviors of the original continuous noisy model [Eq. (3)].

The return time of the periodic point A is calculated by studying the long-time random switching behaviors in the Poincaré section. The mean of the return time of the attractor is calculated for different noise intensity and the result is shown in Fig. 10. As shown in the figure, the mean of the return time decreases with noise intensity D, reaches a minimum, and increases again. The mean of the return time has a minimum value at an optimal value of noise intensity. To compare with stochastic resonance in a classical bistable system, we consider a simple double-well system with weak periodic signal and noise input, this model has been widely studied to account for the basic mechanism of stochastic resonance [24,27]. The return time of one equilibrium state of the model is calculated. As shown in Fig. 11, for the classical bistable system, the mean of the return time decreases monotonically with noise intensity increasing. This is different from our case, which is one aspect that makes our case different from the previous studies about stochastic resonance in the typical bistable system. Here we want to comment about this difference. For the case studied by us, in view of the continuous dynamics of the model, the bistability is dynamic. If a noisy orbit is switched into an attractor, it will move along the attractor for at least a full period of that atractor. The time scale of the motion within the dynamic attractor is comparable to that of the random transitions induced by noise, thus the motion within the attractors cannot be neglected. Moreover, the attractors have different periods and there exists the cooperation of the two dynamic attractors due to noise. For the typical double-well system, the bistability is due to the coexistence of two stable equilibrium points. There is a clear-cut separation of time scales, the time scale of the interwell hopping is much larger than the time scale that characterizes local relaxation within the potential wells. In the approximate theory of stochastic resonance, the intrawell behaviors can be neglected and the mean of the return time decreases as noise intensity increases [28].

The pulse-number distribution $P(n,T)$, which is the probability of the occurrence of n spikes in a fixed time interval T (counting time), can also be used to describe statistical characteristics of neuronal spikes trains [29]. The count mean and the count variance of the pulse-number distribution are calculated from the standard formulas:

$$\overline{n}(T)=\sum_{n=0}^{n_{\max}} np(n,T), \tag{4}$$

$$\sigma^2(T)=\sum_{n=0}^{n_{\max}} n^2p(n,T)-[\overline{n}(T)]^2. \tag{5}$$

The mean-to-variance ratio $R(T)$ is defined as

$$R(T)=\overline{n}(T)/\sigma^2(T). \tag{6}$$

For our case [Eq. (3)], the pulse-number distribution has a bell-shaped structure as shown in Fig. 12. Here the counting time $T=12$ is used to calculate the pulse-number distribution. Since the forced FHN model studied by us displays both monostable and bistable regimes, we will study how the mean-to-variance ratio changes when the system moves from one regime to the other and show the difference between the case studied here and the previous studies about stochastic resonance in the excitable neuron model. First, the mean-to-variance ratios for different noise intensity are calculated for the case of $b=0.23$, $r=0.0292$, in this case the forced FHN neuron model has only one stable subthreshold oscillation. The mean-to-variance ratios $R(T)$ versus noise intensity are shown in Fig. 13(a). As shown in the figure, $R(T)$ decreases monotonically with noise intensity D increasing. Then the mean-to-variance ratios are calculated for the case of $b=0.245$, $r=0.0292$, which is close to the boundary separat-

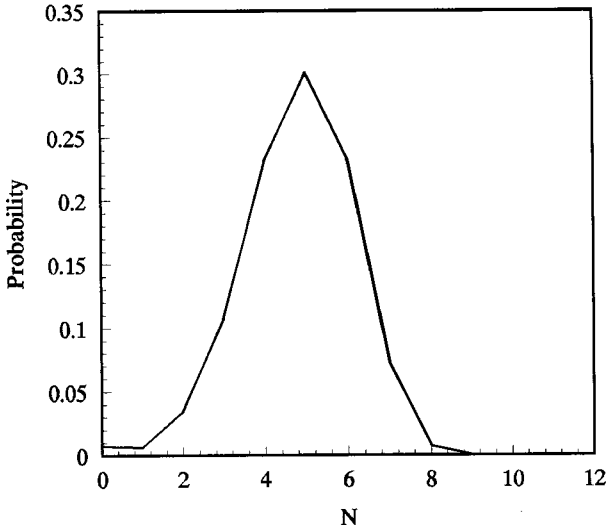

FIG. 12. The pulse-number distribution for Eq. (3), parameter $a=0.2466$, $b=0.0292$, when the noise intensity $D=4\times10^{-7}$. The units of the axes are arbitrary.

ing the monostable and the bistable regimes. The results are shown in Fig. 13(b). We can see that $R(T)$ decreases with noise intensity D, reaches a minimum, and increases again. Finally, for the case studied here, $b=0.2466$, $r=0.0292$, the forced excitable system has both subthreshold and suprathreshold oscillations. The results about mean-to-variance ratios versus noise intensity for the case are calculated and shown in Fig. 13(c). As shown in the figure, $R(T)$ increases monotonically with noise intensity D increasing. We can verify that stochastic resonance can occur for the excitable FHN neuron model with $b=0.23$, $r=0.0292$, and this case is similar to the previous study about stochastic resonance in the excitable model [5,25]. In their consideration, the forced FHN excitable model also has one stable subthreshold oscillation. From the above calculations, we can see that the mean-to-variance ratios versus noise intensity have different forms for the model in the monostable and the bistable regimes, and in the process of the change from the monostable to the bistable regimes, the mean-to-variance ratios versus noise intensity undergo an intermediate process shown in Fig. 13(b). Thus the values of the mean-to-variance ratios of the pulse-number distribution can serve to show the difference between the case studied by us and the previous studies about stochastic resonance in the excitable neuron model.

Besides the differences pointed out in the above studies, for our case the amplitude of the external input periodic signal is much weaker than that of the previous case [5]. For the purpose of detecting the weak external signal in the nervous system, our studied case could be of interest for real sensory neurons. Here we should note that, in our studies, because the subthreshold oscillation and the suprathreshold oscillation can be generated simultaneously by the external stimulation, the external signal can be regarded as a suprathreshold stimulation as well as a subthreshold stimulation. Our studies extend the classical stochastic resonance which is used to detect a subthreshold signal to a new range that can be used to detect a suprathreshold signal for neurons.

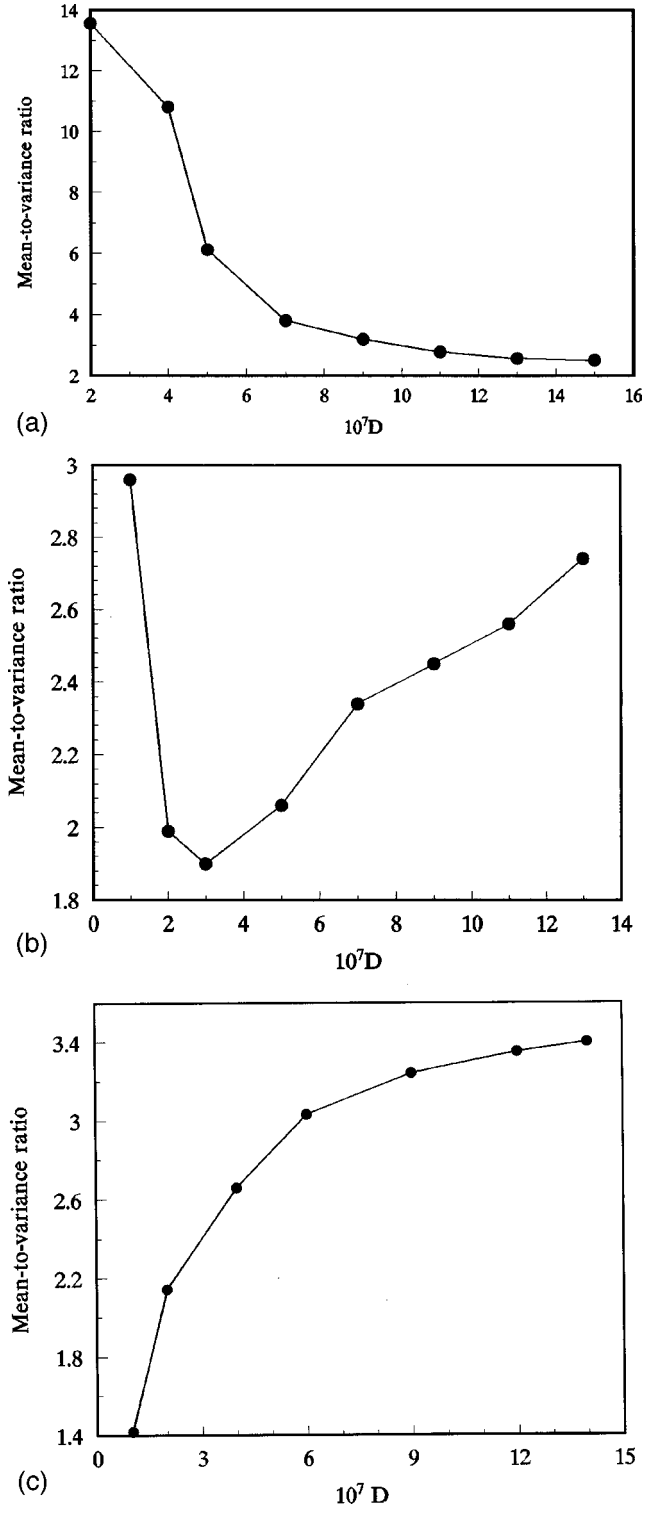

FIG. 13. Mean-to-variance ratios versus noise intensity for the cases: (a) $b=0.23$, $r=0.0292$; (b) $b=0.245$, $r=0.0292$; and (c) $b=0.2466$, $r=0.0292$. The counting time $T=12$. The units of the axes are arbitrary.

III. THE FRACTAL BASIN BOUNDARY AND THE STABILITY OF NEURONAL FIRINGS

In the shadowed regions of Fig. 2, which show the coexistence of stable periodic oscillations, we choose the param-

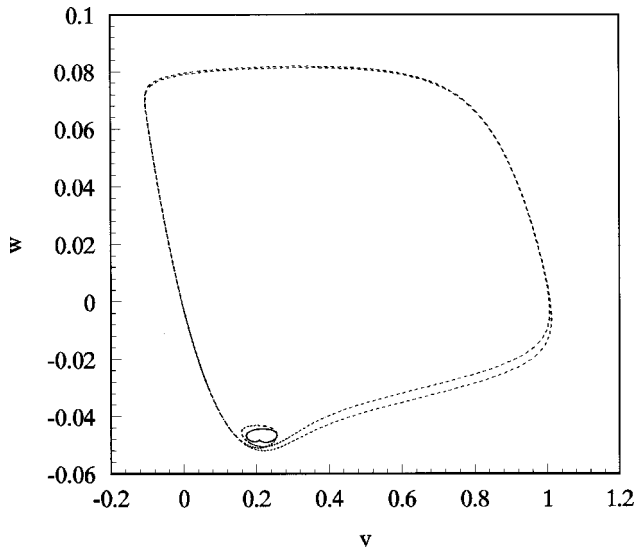

FIG. 14. The subthreshold small-amplitude periodic solution with period $T_1=T_0$ and the suprathreshold large-amplitude periodic solution with period $T_2=3T_0$, when parameter $b=0.259\,92$, $r=0.0163$. The dashed line is for the suprathreshold oscillation and the solid line is for the subthreshold oscillation. The units of the axes are arbitrary.

eter $b=0.259\,92$, $r=0.0163$. For this case, Eq. (1) has the small-amplitude subthreshold periodic oscillation with period $T=T_0$ and the large-amplitude suprathreshold oscillation with period $T=3T_0$. They are shown in Fig. 14. The basin of attraction for the case can be obtained by the same method as the one used in the above section. Figure 15 shows the basin of attraction in the phase space. The figure exhibits that the basin boundary between the two coexistent attractors has a fractal structure, and this is verified by the

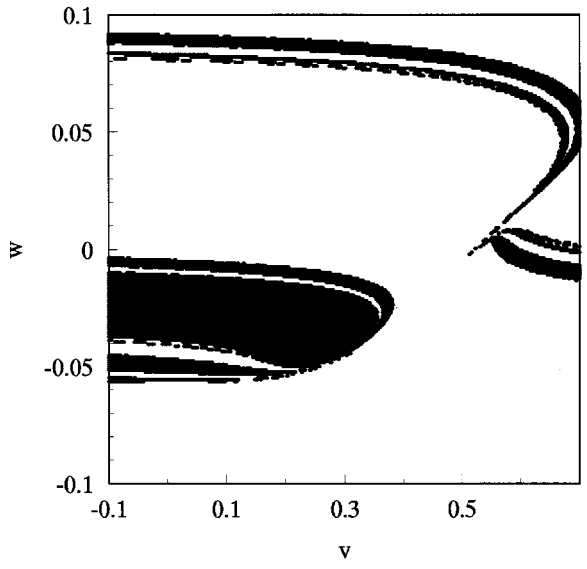

FIG. 15. Basin of attraction for the forced FHN neuronal model when $b=0.259\,92$, $r=0.0163$. The black dots represent the basin of attraction of the subthreshold oscillation, the other region is the basin of attraction of the suprathreshold oscillation. The units of the v and w are arbitrary.

further calculation about the dimension of the basin boundary. The dimension of the basin boundary is calculated by the method presented in [30]. In the phase space we choose 400×200 uniform distribution initial conditions over the region of $-0.1<v<0.7$, $-0.1<w<0.1$ and integrate each one to determine its final state. Each initial condition (v_0,w_0) is then perturbed in the horizontal direction by $\pm\varepsilon$ to produce two perturbed initial conditions $(v_0\pm\varepsilon,w_0)$, all 160 000 perturbed initial conditions are iterated to determine their basins, if either of the two perturbed initial conditions associated with a particular unperturbed initial condition is in a basin different from the unperturbed one, we say that the initial condition is uncertain under the error ε, and the fraction of the uncertain initial conditions $f(\varepsilon)$ is recorded. The uncertain fraction $f(\varepsilon)$ satisfies $f(\varepsilon)\sim\varepsilon^{\alpha}$. The uncertainty exponent α is related to the basin boundary capacity dimension d, $d=D_0-\alpha$, where D_0 is the dimension of the phase space, $D_0=2$. By the above method, we can obtain that the capacity dimension of the basin boundary is $d=1.32$.

It is generally regarded that fractal basin boundary is generated by the homoclinic intersection of the stable and unstable manifold of a saddle orbit [30–32]. For the case studied by us we first study the main global bifurcation near the parameter $b=0.259\,96$. We fixed $r=0.0163$ and let b vary. When $b=0.2595$ the periodically forced FHN neuronal model has only one stable subthreshold periodic oscillation with period T_0. As b is increased to $b=0.2596$, a stable periodic oscillation with T_0 and a saddle periodic oscillation with period $T=3T_0$ begin to appear. Here the unstable periodic solution is detected by the Newton-Raphson method. A saddle-node bifurcation occurs at $b=0.2596$. When $b>0.2596$, the system has the two coexistent stable attractors, one is the subthreshold oscillation with period T_0, the other is the stable suprathreshold oscillation generated by the saddle-node bifurcation. This type of saddle-node bifurcation occurring at $b=0.2596$ is referred to as a supercritical saddle-node bifurcation [33]. The saddle orbit generated by the saddle-node bifurcation still exists at $b=0.259\,96$, and the homoclinic tangles of the stable and the unstable manifold of the saddle orbit result in the appearance of the fractal basin boundary. The homoclinic tangles of the stable and the unstable manifold of the saddle orbit can be obtained by calculating the stable and unstable manifold of the saddle orbit using the methods presented in [34].

In the nervous system, since information may be encoded by the interspike intervals of neuronal firings, the state of neuronal firings has great meaning for neurons. When neurons are in a nonfiring state, the neurons do not generate firings. But for the firing state, neurons can generate spike trains which are accepted by other neurons, and information encoded in the intervals between these spikes is transmitted to other neurons. The firing states can be periodic or irregular. For the periodic firing state, the intervals between the firings of neurons have an equivalent value. For chaotic and random firing states, the intervals of the neurons firings are irregular. A precondition of the interspike intervals code is that the firings in response to an input signal be stable in the presence of noise. It is necessary to study the stability of neuronal firings under noise perturbations. For a given inten-

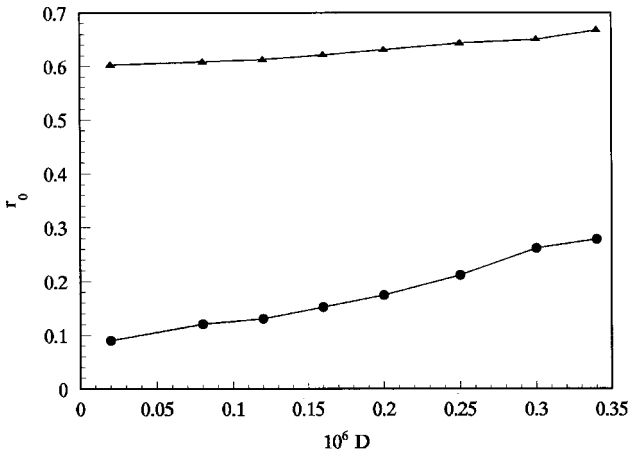

FIG. 16. r_0 versus the noise intensity for the cases: (a) $b=0.259\,92$, $r=0.0163$ (triangles) and (b) $b=0.2466$, $r=0.0292$ (dots). The units of the axes are arbitrary.

sity of noise, if neuron firings do not transit from a firing state to a subthreshold nonfiring state or to another firing state, then it is regarded to be stable. Otherwise, it is regarded to be unstable.

In the present study when external noise perturbation is also forced on the neuron model we discuss whether the stability of the firing state is related to the global dynamics of the neuron model. We study the above two cases, one with parameter $a=0.2466$, $r=0.0292$, as shown in Fig. 4, the basin boundary is smooth. The other with parameter $a=0.259\,96$, $r=0.0163$, as shown in Fig. 15, the basin boundary is fractal. Because the magnitude of Gaussian distributed perturbation is unbounded, transitions from one state to another will always be possible. For practical purposes, the effect of noise on the stability of the neuron firings is considered in a given time. In the present study, the given time interval is chosen as $t=100\,000$. For the two cases, as studied in the above section, in the region $-0.1<v<0.7$, $-0.1<w<0.1$, 400×200 initial points are uniformly chosen to study their basin of attraction. Each one of the initial points that start from the basin of attraction of the firing state (the suprathreshold oscillation) is perturbed by noise [Eq. (3)]. In the given time interval $t=100\,000$, if the point does not transit from the firing state to the subthreshold nonfiring state, the firing state of the initial point is regarded to be stable under external noise perturbation, otherwise it is regarded to be unstable. The value $r_0=N_u/N_0$ is used to quantify the sensitivity of firing state to noise, where N_0 is the number of initial points in the basin of the suprathreshold oscillation which can generate firings and N_u is the number of the initial points which are unstable under noise perturbation. For the two cases, the relative quantity r_0 versus noise intensity are calculated and shown in Fig. 16. Comparing the two cases shown in Fig. 16, we can obtain that, for the neuron model with fractal basin boundary, noise perturbation can induce many more initial points to change from the firing state to the nonfiring state than that with smooth basin boundary, and for the case with the fractal basin boundary the stability of the firing state can be changed easily. This phenomenon can be understood in terms of the state of the basin of attraction. For the systems with basin boundary separating the basins of coexisting attractors, the uncertain fraction $f(\varepsilon)$ of initial conditions which are sensitive to small perturbation ε obey $f\sim\varepsilon^{\alpha}$ [30], where α is the uncertain exponent. For the case of $a=0.259\,96$, $r=0.0163$, the basin boundary is fractal and the fractal dimension of the basin boundary $d=1.32$, and the uncertain exponent $\alpha=D-d=0.68$. The uncertainty exponent is significantly less than one. But for the case $a=0.2466$, $r=0.0292$, the basin boundary is smooth, and the uncertain exponent $\alpha=1$. We can obtain that the uncertainty fraction f of the case with fractal basin boundary is much more than that of the case with smooth basin boundary. So, the case with fractal basin boundary noise can induce many more points to transit from the firing state to the subthreshold nonfiring state, and noise can change the stability of the firing state easily. When $a=0.259\,96$, $r=0.0163$ the system has the fractal basin boundary, we also can observe that if a trajectory is perturbed into boundary it will undergo transient chaotic motion before setting on one of the periodic attractors as in Refs. [35], [36]. This phenomenon will increase the complexity of the system [36], and the complexity that arises in this typical neuron model with noise perturbations might provide insight for interpreting some complex behaviors of neurons.

IV. CONCLUSION

In summary, we show that the small-amplitude subthreshold periodic oscillation and the large-amplitude suprathreshold periodic oscillation coexist commonly in some parameter regions of the forced excitable FHN neuron model. We also find that the random transitions induced by noise between the subthreshold oscillation and the suprathreshold oscillation are the essential mechanism underlying stochastic resonance studied by us. This kind of bistability was also found in the Hodgkin-Huxley neuron model with time-dependent sinusoidal stimulation [37], but stochastic resonance was discussed only in the region where the periodically forced Hodgkin-Huxley neuron model has one attractor, a stable nonfiring state. It is no doubt that the appearance of such dynamic bistability should exist in other forced excitable neuronal models such as the Morris-Lecar neuron model and the Chay neuron model. Moreover, such bistability has been observed experimentally in neurons. Therefore our results may help us to understand stochastic resonance in these neuron systems.

In comparison with the previous studies about stochastic resonance, our work shows that stochastic resonance of the excitable neuronal model is related to the dynamic bistability. Furthermore, the transitions induced by noise between the two dynamic oscillation are studied by us. The mean of the return time and the mean-to-variance ratio of the pulse-number distributions are calculated in our works, the results suggest that these values can serve to distinguish our case from the previous studies about stochastic resonance in the typical bistable nonlinear system and the excitable neuronal model. Moreover, it is interesting to note that for our case the external signal can be regarded not only as a subthreshold stimulation but also a suprathreshold stimulation, thus our

studies also extend the classical stochastic resonance which is used to detect a subthreshold signal to a new range that can be used to detect suprathreshold signal for neurons.

Through comparing the stability of the firings of the FHN neuron model with smooth basin boundary and that with fractal basin boundary, we can draw the conclusion that the stability of firings of the forced FHN neuron with fractal basin boundary can be changed easily under the small noise perturbation. This result suggests that in order to maintain the stability of firing state subjected to random perturbations, the neuron model should be operated in the region where the basin of attraction is smooth. The result also suggests that when we study the dynamic behaviors of some typical neuronal models, much attention should be paid to the global dynamics of these systems. As shown in the present studies, the global characteristics may have significant effects on some issues we are interested in.

ACKNOWLEDGMENT

This work was supported by NSFC Grant Nos. 19972051 and 39970242.

[1] M. C. Cross and P. C. Hobenberg, Rev. Mod. Phys. **65**, 851 (1993).
[2] L. Glass and M. C. Mackey, *From Clocks to Chaos: The Rhythm of Life* (Princeton University, Princeton, NJ, 1988).
[3] R. FitzHugh, in *Biological Engineering*, edited by H. P. Schwann (McGraw-Hill, New York, 1962); J. Nagumo, S. Arimoto, and S. Yoshizawa, Proc. IRE **50**, 2061 (1962).
[4] J. C. Alexander *et al.*, SIAM (Soc. Ind. Appl. Math.) J. Appl. Math. **50**, 1373 (1990).
[5] A. Longtin, J. Stat. Phys. **70**, 309 (1993).
[6] K. Wiesenfeld *et al.*, Phys. Rev. Lett. **72**, 2125 (1994).
[7] J. P. Baltanas and J. M. Casado, Physica D **122**, 231 (1998).
[8] J. J. Collins, C. C. Show, and T. T. Imhoff, Phys. Rev. E **52**, 2988 (1995).
[9] A. Longtin and D. R. Chialvo, Phys. Rev. Lett. **81**, 4012 (1998).
[10] X. Pei, K. Bachman, and F. Moss, Phys. Lett. A **206**, 61 (1996).
[11] A. S. Pikovsky and J. Kurths, Phys. Rev. Lett. **78**, 775 (1997).
[12] S. W. Hughes *et al.*, J. Physiol. (London) **517**, 805 (1999).
[13] D. A. Baxter, J. W. Clark, and J. H. Byrne, J. Neurophysiol. **75**, 957 (1996).
[14] K. Kopeczk *et al.*, Biol. Cybern. **69**, 463 (1993).
[15] S. Coombes, Phys. Lett. A **255**, 49 (1999).
[16] F. Rieke, *Spikes, Exploring the Neural Code* (MIT, Cambridge, MA, 1997).
[17] G. Decon and B. Schurmann, Phys. Rev. Lett. **79**, 4697 (1997).
[18] W. Calvin and C. Stevens, J. Neurophysiol. **31**, 574 (1968).
[19] J. Guckenheimer and P. Holmes, *Nonlinear Oscillations, Dynamical Systems and Bifurcation of Vector Fields* (Springer-Verlag, Berlin, 1983).
[20] B. Barnes and R. Grimshaw, J. Aust. Math. Soc. B, Appl. Math. **38**, 427 (1997).
[21] B. Barnes and R. Grimshaw, Int. J. Bifurcation Chaos Appl. Sci. Eng. **7**, 2653 (1997).
[22] R. Benzi, S. Sutera, and A. Vulpiani, J. Phys. A **14**, L453 (1981).
[23] K. Wiesenfeld and F. Moss, Nature (London) **373**, 33 (1995).
[24] A. Longtin, S. Bulsara, and F. Moss, Phys. Rev. Lett. **67**, 656 (1991).
[25] S. R. Massanes and C. J. P. Vicente, Phys. Rev. E **59**, 4490 (1999).
[26] M. H. Choi, R. F. Fox, and P. Jung, Phys. Rev. E **57**, 6335 (1998).
[27] T. Zhou and F. Moss, Phys. Rev. A **42**, 3161 (1990).
[28] L. Gammaitoni, P. Hanggi, P. Jung, and F. Marchesoni, Rev. Mod. Phys. **70**, 223 (1998).
[29] M. C. Teich and S. M. Khanna, J. Acoust. Soc. Am. **77**, 1110 (1985).
[30] S. W. Mcdonald, C. Grebogi, E. Ott, and J. A. Yorke, Physica D **17**, 125 (1985).
[31] F. C. Moon and G. X. Li, Phys. Rev. Lett. **55**, 1439 (1985).
[32] M. S. Soliman and J. M. T. Thompson, Phys. Rev. A **45**, 3425 (1992).
[33] J. K. Hale, *Dynamics and Bifurcations* (Springer-Verlag, New York, 1991).
[34] T. S. Parker and L. O. Chua, *Practical Numerical Algorithms for Chaotic Systems* (Springer-Verlag, Berlin, 1989).
[35] M. Iansiti, Q. Hu, R. M. Westervelt, and M. Tinkham, Phys. Rev. Lett. **55**, 746 (1985).
[36] L. Poon and C. Grebogi, Phys. Rev. Lett. **75**, 4023 (1995).
[37] S. G. Lee and S. Kim, Phys. Rev. E **60**, 826 (1999).